Allosteric Modification, the Primary ATP Activation Mechanism of Atrial Natriuretic Factor Receptor Guanylate Cyclase

ARTICLE *in* BIOCHEMISTRY · FEBRUARY 2011

Impact Factor: 3.02 · DOI: 10.1021/bi1018978 · Source: PubMed

3 AUTHORS, INCLUDING:

Teresa Duda
Salus University
105 PUBLICATIONS **2,620** CITATIONS
SEE PROFILE

Rameshwar K Sharma
Salus University
193 PUBLICATIONS **3,986** CITATIONS
SEE PROFILE

Published in final edited form as:
Biochemistry. 2011 February 22; 50(7): 1213–1225. doi:10.1021/bi1018978.

Allosteric Modification, the Primary ATP Activation Mechanism of ANF-RGC

Teresa Duda[*], **Prem Yadav**, and **Rameshwar K. Sharma**
Research Divisions of Biochemistry and Molecular Biology, The Unit of Regulatory and Molecular Biology, Salus University, 8360 Old York Road, Elkins Park, PA 19027, USA

Abstract

ANF-RGC is the prototype receptor membrane guanylate cyclase being both the receptor and the signal transducer of the most hypotensive hormones, ANF and BNP. It is a single transmembrane-spanning protein. After binding these hormones at the extracellular domain it at its intracellular domain signals activation of the C-terminal catalytic module and accelerates the production of its second messenger, cyclic GMP, which controls blood pressure, cardiac vasculature and fluid secretion. ATP is obligatory for the post-transmembrane dynamic events leading to ANF-RGC activation. It functions through the ATP regulated module, ARM (KHD) domain, of ANF-RGC. In the current over-a-decade-held-model "phosphorylation of the KHD is absolutely required for hormone-dependent activation of NPR-A" (Potter, L.R., and T. Hunter. 1998. Mol. Cell. Biol. 18: 2164–2172). The presented study challenges this concept. It demonstrates that, instead, ATP allosteric modification of ARM is the primary signaling step of ANF-GC activation. In this 2-step new dynamic model, ATP in the first step binds ARM. This triggers in it a chain of transduction events, which cause its allosteric modification. The modification partially activates (about 50%) ANF-RGC; and concomitantly also prepares the ARM for the second successive step. In this second step, ARM is phosphorylated and ANF-RGC achieves additional (~50%) full catalytic activation. The study defines a new paradigm of ANF-RGC signaling mechanism.

Keywords

ANF receptor guanylate cyclase; cyclic GMP; ATP allosteric regulation; signal transduction; phosphorylation; cardiac vasculature

---

In the first chapter, the discovery of ANF-RGC, the first member of the membrane guanylate cyclase family, demonstrated that a striking feature of this family is that it is also a receptor of the natriuretic peptide hormones, ANF-RGC being the receptor of ANF (1–5). Later studies showed that it is also a physiological receptor of another peptide hormone, BNP (6). With the inclusion of two other members--CNP-RGC, the receptor of C-type natriuretic peptide (CNP) (7,8) and STa-RGC, the receptor of heat-stable enterotoxin, guanylin and uroguanylin (9–11), the peptide hormone receptor guanylate cyclase family expanded to three members. These members have also been respectively termed as GC-A, GC-B, and GC-C (reviewed in: 12).

A second chapter in the membrane guanylate cyclase transduction field was unfolded with the discovery of the photoreceptor guanylate cyclase, ROS-GC, presently referred to as ROS-GC1 (13,14). ROS-GC, present in rod and cone outer segments, one of the central

Corresponding authors: Rameshwar K. Sharma, rsharma@salus.edu, phone: 215-780-3124, fax: 215-780-3125. Teresa Duda, tduda@salus.edu, phone: 215-780-3112, fax: 215-780-3125.

components of the phototransduction machinery, was not a surface receptor of any peptide hormone but was solely modulated by the intracellular levels of free Ca^{2+}. Ca^{2+} was captured by the Ca^{2+}-sensor proteins, GCAPs and CD-GCAPs, which controlled the activity of ROS-GC (reviewed in: 15). Thus, the membrane guanylate cyclase family branched into two subfamilies, peptide hormone receptor and Ca^{2+}-modulated ROS-GC. And the family became the transducer of both types of signals, generated outside and inside the cells. Presently, the ROS-GC subfamily consists of three members—ROS-GC1, ROS-GC2, and ONE-GC, they have alternately been termed as GC-E, GC-F, and GC-D, respectively (reviewed in: 12,16–19). A unique functional theme of this subfamily is that at its intracellular domain through GCAPs and CD-GCAPs it is delicately modulated by the levels of intracellular free Ca^{2+} concentrations.

Recently, a third chapter has unfolded in the field with the discovery that the Ca^{2+}-modulated odorant-linked ONE-GC is also a receptor of an extracellular odorant ligand, uroguanylin (20,21). Thus, this guanylate cyclase is the sole representative of a new subfamily, which is a hybrid of the peptide hormone receptor and ROS-GC subfamilies. Remarkably, this subfamily, unlike its parent ROS-GC subfamily, is positively modulated by the Ca^{2+}-sensor GCAP1 (22) and is also the transducer of atmospheric $C0_2$ (23,24). The mechanism for this signal transduction does not involve either its extracellular or intracellular domain, it directly involves its catalytic domain (23).

A common structural trait of the membrane guanylate cyclase family is that all its members are single transmembrane-spanning proteins, composed of modular blocks (reviewed in: 12). Functionally, they are homo-dimeric. In each mono-meric subunit, the transmembrane module divides the protein into two roughly equal portions, extracellular and intracellular. The individual modules within each portion provide functional uniqueness to each member of the guanylate cyclase family. Each modular block within the extracellular region of the receptor guanylate cyclases uniquely senses its peptide hormone signal and within the intracellular block of a ROS-GC its Ca^{2+} signal. The catalytic domain in each membrane guanylate cyclase resides in its intracellular region. Importantly, with a distinctive characteristic, the core catalytic domain of ROS-GC1 is also directly modulated by the Ca^{2+}-sensor neurocalcin δ (25). The topographical arrangement of this domain also differs in the two sub-families. In the peptide hormone receptor, it is at the C-terminal end and in the ROS-GC it is followed by a C-terminal extension (reviewed in: 12). Similar topology holds for the third subfamily member, ONE-GC.

Like ANF-RGC, its ligand hormone, ANF is a prototype of the natriuretic peptide family (26; reviewed in: 27,28). Gene knockout studies link ANF and ANF-RGC with salt-sensitive (29) and salt-in-sensitive hypertension (30), cardiac hypertrophy and vascular fibrosis (31). Thus, ANF and ANF-RGC are critical components of the renal and cardiovascular physiology.

In the current two-step dynamic ANF-RGC activation model [Fig. 7 in (32)] the post-transmembrane ANF signaling events are controlled by ATP through the ARM (ATP-regulated) domain. ANF-RGC in its basal state exists as a dimer. The signaling process is initiated by the binding of ANF to the extracellular domain of ANF-RGC (12). One molecule of ANF binds to the extracellular dimer (34,35). The binding modifies and twists the hinge juxtamembrane region and induces the structural change in the ARM domain (34,36–38), allowing it to bind ATP in the *first-step*. The cyclase activity remains at its basal level. Upon interaction with its binding pocket, ATP induces a cascade of temporal and spatial changes in the entire ARM domain (39,40; reviewed in: 41–43). The cyclase is partially activated (32). In the *second step*, through an unknown mechanism, the six serine/threonine residues within the ARM domain become phosphorylated (44,45) and ANF-RGC

becomes fully active (32). It has been established that the activation of the catalytic module occurs through the ARM ^{660}WTAPELL^{675} motif (39).

The present study focuses on the liaison between the *first* and the *second step* of the model. It dissects the events of ATP allosteric effect and phosphorylation and challenges the current dogma that considers phosphorylation of the ARM domain the primary requirement for hormone-dependent activation of ANF-RGC (44,45; reviewed in: 46). The study proposes an alternative mechanism where ATP allosteric modification of the ARM domain provides the spatial conditions for the phosphorylation step. These results are explained in a simulated 3-dimensional model.

EXPERIMENTAL PROCEDURES

Materials

ATP, ATPγS and AMP-PNP were purchased from Roche, ANF from Bachem AG, 8-azido-ATP from Affinity Photoprobes, Inc., and staurosporine from Sigma.

Mutagenesis

Point mutations were introduced to ANF-RGC using Quick-change mutagenesis kit (Stratagene) and appropriate mutagenic primers.

Expression in COS cells

COS-7 cells were transfected with ANF-RGC or its mutants' cDNA using a calcium-phosphate coprecipitation technique (47). Sixty hours after transfection, the cells were harvested and their membranes prepared (32,39).

Guanylate cyclase activity assay

Membranes of COS cells expressing ANF-RGC or its mutants were assayed for guanylate cyclase activity in an assay mixture consisting of 10 mM theophylline (phosphodiesterase inhibitor), 15 mM phosphocreatine, 20 μg creatine kinase, 50 mM Tris-HCI, pH 7.5, and ANF, ATP, ATPγS, AMP-PNP or staurosporine. The total assay volume was 25 μl. The reaction was initiated by the addition of the substrate solution containing 4 mM $MgCl_2$ and 1 mM GTP, continued for 10 min at 37 °C, and terminated by the addition of 225 μl of 50 mM sodium acetate buffer (pH 6.25) followed by heating in a boiling water-bath for 3 min. The amount of cyclic GMP formed was quantified by radioimmunoassay (48). All experiments were done in triplicate.

Expression and purification of ANF-RGC ARM domain and its mutants

The ARM domain, aa 486–692, was amplified from ANF-RGC cDNA by PCR and directly cloned into the ligation independent site of pET-30aXa/LIC vector (Novagen). ARM-6A and ARM-6D mutant expression constructs were prepared identically except that the ANF-RGC-6A and ANF-RGC-6D cDNAs were used for amplification of the ARM, aa 486–692 fragment by PCR. The proteins were expressed and purified by FPLC. The majority (80%) of each protein was monomeric (the collected fraction), only about 15% was in a form of high molecular mass aggregates eluting in the void volume; minor degradation products of low molecular weight were also observed.

UV cross-linking

According to the previous protocol (32,39,49), 1 μg (50 pmol) of the purified protein (ARM domain or its 6A or 6D mutants) in 20 mM phosphate buffer pH 7.5 was incubated for 5 min with 100 pmol of 8-azido-ATP, 1 μCi [γ^{32}P]-8-azido-ATP (specific activity 10–15 Ci/

mmol), 1 mM $MgCl_2$ and ATP in a total volume of 25 μl. The reaction mixture was UV irradiated (254 nm) and analyzed by SDS-15%PAGE followed by autoradiography and liquid scintillation counting.

Molecular modeling

The 3-dimensional structure of the ANF-RGC ARM domain in its apo-form and ATP bound states (PDB file 1T53) was used for the mutant modeling. The residues S^{497}, T^{500}, S^{502}, S^{506}, S^{510}, and T^{513} were mutated to alanine or aspartate in both apo and ATP bound structures. In each case the side chains were scanned to minimize bad contacts and optimize favorable interactions with the surrounding residues. The final structures were energy refined using Kollman united charge and force field and maximin2 minimizer of SYBYL molecular modeling package (Tripos Associates) for 100 iterations. Electrostatic potentials at the surface of the ANF-RGC ARM domain for the apo enzyme and for the mutants were calculated using Kollman united charge and SYBYL modeling package.

RESULTS

ATP allosteric modification of ARM is the first step in ANF-RGC activation

Background—Based on sequence identity with the tyrosine protein kinases the part of the intracellular domain preceding the, at that time, ill-defined boundary of the catalytic (Cat) domain was named the Kinase Homology Domain (KHD) of ANF-RGC (33,50; reviewed in: 12,41). The boundaries of the Cat and KHD have since been functionally defined; consequently, KHD has been renamed functionally as ARM domain (ATP-regulated domain) [reviewed in: 12,41; the early studies starting from the discovery of ATP regulation in 1991 to the defining of the biochemical and structural principles of the ARM domain have been covered in a comprehensive review (42)]. Within its structure, ARM domain contains a Glycine-rich cluster (Grc) (51), which is meshed in and flanked by six phosphorylation sites, four serines and two threonines (45,52) (Fig. 1A). The six phosphorylation sites together with Grc, constitute critical signaling motif of ATP. Very recently, seventh phosphorylation site has been identified (53,54). This site however, appears to be rather involved in the desensitization of ANF-RGC (53). The present consensus is that “phosphorylation of KHD is absolutely required for hormone-dependent activation of NPR-A” (45,52; reviewed in: 46). Without KHD phosphorylation, ANF-RGC and CNP-RGC are totally desensitized (44,45,52,55). In this concept, a hypothetical protein kinase co-exists with ANF-RC in the plasma membranes (56). It transfers the terminal phosphate group of ATP to these six ARM phosphorylation sites, causing ANF-RGC (and CNP-RGC) to be phosphorylated and activated (44,45,52,55,56). Another important constituent believed to co-exist with the protein kinase and ANF-RGC is a hypothetical phosphatase, which dephosphorylates the six phosphorylated residues (56).

In the present investigation, the above concept was tested using two approaches, biochemical and molecular modeling. In the biochemical approach, among others, the recently developed staurosporine probe that mimics ATP in allosteric modification of the ARM domain (32) was used; through molecular modeling, the ATP-dependent changes in the stereo orientation of the side chains of the phosphorylated residues were analyzed.

In the first task, the six serine and threonine residues in the ARM domain of ANF-RGC (Fig. 1) were converted to alanine. This resulted in the construction of ANF-RGC-6A mutant, which can no longer be phosphorylated, thus, this mutant represented the dephosphorylated form of ANF-RGC (Fig. 1B). In the second task, the six residues were converted individually to alanine, resulting in the construction of six mutants, each containing one of the following mutations: $S^{497}A$, $T^{500}A$, $S^{502}A$, $S^{506}A$, $S^{510}A$, or $T^{513}A$.

These mutants were analyzed to assess the role of each residue in the ANF/ATP-dependent activation of ANF-RGC.

The wt-ANF-RGC and ANF-RGC mutants are properly expressed in the heterologous expression system of COS cells—Before the mutants could be used for the study designed, it was critical to verify that in the heterologous expression system of COS cells they are properly and comparably to the wt-ANF-RGC expressed in the cell membranes and that they have retained their structural integrity.

The wt-ANF-RGC and the mutants were individually expressed in COS cells, their membrane fractions were prepared, and the guanylate cyclase activities determined. The basal guanylate cyclase activity of all the mutants and wt-ANF-RGC was comparable, ranging from 4 to 6 pmol cyclic GMP formed minute^{-1} mg^{-1} protein. Membranes of "mock" transfected COS cells showed very low guanylate cyclase activity, 0.3 pmol cyclic GMP formed minute^{-1} mg^{-1} protein. That the guanylate cyclase activities in the membranes of transfected cells correlated with the proteins' expression levels was validated through Western-blot analyses. The immunoreactive bands had comparable intensities (Fig. 2). It was, thus, concluded that the individual and combined six Ala mutations did not affect the expression and guanylate cyclase activity of the mutant proteins.

To assure that the mutants have retained their structural integrity, the K_m values for the substrate GTP of ANF-RGC-6A mutant, the single A mutants and of the wt-ANF-RGC were compared. They were comparable, ranging from 480–510 μM GTP (Table 1). Hence, the mutations had no effect on the structural integrity of the guanylate cyclases, their basic structures remained intact.

To determine if ATP allosterically modulates the dephoshorylated form of ANF-RGC the recently developed staurosporine probe (32) was used first. Staurosporine mimics ATP in allosteric modification of ARM, its effect is independent of phosphorylation and results in partial activation of ANF-RGC (32).

Membranes of COS cells individually expressing wt-ANF-RGC, the dephosphorylated forms of ANF-RGC and the ANF-RGC alanine mutants were exposed to 10^{-7} M ANF in the presence of increasing (10 nM to 10 μM) concentrations of staurosporine. In the control experiments, the membranes were exposed to 10^{-7} M ANF only. ANF-alone stimulated ANF-RGC activity minimally, up to ~10 pmol cyclic GMP min^{-1} mg protein^{-1}. In the presence of ANF and staurosporine, wt-ANF-RGC activity was stimulated in a dose-dependent fashion (Fig. 3A). Half-maximal stimulation was observed at 50 nM staurosporine and the V_{max} of 4.3-fold above basal activity was observed at 1 μM. In accordance with the earlier conclusions (32), these results demonstrate that staurosporine mimics ATP-dependent allostric effect, and that this effect is independent of the phosphorylation of ANF-GC.

To determine whether staurosporine in addition to increasing V_{max} of ANF-RGC affects also its K_m for GTP, membranes of COS cells expressing wt-ANF-RGC were exposed to varying concentrations of GTP (Mg^{2+} cofactor) and constant 10^{-7} M ANF with or without 1 μM staursporine. In parallel control experiment, 1 mM AMP-PNP instead of staurosporine was used. AMP-PNP was used as control because previous results have shown that the staurosporine effect on ANF-dependent activity of ANF-RGC is virtually identical to that of AMP-PNP (32). As evident from figure 3B, both staurosporine and AMP-PNP lower the K_m of ANF-RGC for GTP. This decrease is from 0.5 mM (the K_m in the absence of staurosporine or AMP-PNP) to 0.07 mM GTP in the presence of staurosporine and to 0.06 mM GTP in the presence of AMP-PNP as determined from fitting the dose-response curves

to the Hill's equation). Thus, staurosporine and AMP-PNP affect both the kinetic parameters of ANF-RGC, V_{max} and K_m.

Virtually identical results were obtained with ANF-RGC-6A and the six individual-A mutants: $S^{497}A$; $T^{500}A$; $S^{502}A$; $S^{506}A$; $S^{510}A$; and $T^{513}A$. In all cases, staurosporine signaled ANF stimulation of ANF-RGC (Fig. 4A–G). The stimulation was staurosporine dose-dependent and the maximal stimulation of 4 to 5-fold over the basal activity was achieved at ~1 μM staurosporine. The staurosporine EC_{50} values estimated from the dose-dependence graphs were at approximately 50 nM (Fig. 4). The calculated Hill coefficient for all the dose-response curves was 1 ± 0.15, indicating non-cooperative binding of staurosporine to ANF-RGC and its mutants. The EC_{50} values derived from Hill'plots for the wt ANF-RGC and the mutants were between 20 and 30 mM. Thus, the graphically estimated and the calculated EC_{50} values are comparable.

These results indicate that the ATP-dependent allosteric modification and stimulation of ANF-RGC activity is independent of the phosphorylation state of ANF-RGC.

Studies with adenine nucleotides further validated these conclusions—There was a riddle in the original studies, which linked ATP with the ANF/ANF-RGC signaling (57,58). This was that AMP-PNP a non-hydrolyzable analogue of ATP was only about half as effective as ATP in stimulating ANF-RGC. ATPγS was the most effective, causing about 30% additional saturation of enzymatic activity over ATP. The proposed explanation for the excessive ATPγS effect was that it exhibited two ATP activities: one, being a substrate for a hypothetical protein kinase bound to ANF-RGC, two, acting as an allosteric modifier of ANF-RGC. In addition, the thiophosphate group was not a substrate for a hypothetical phosphatase, co-present with a hypothetical protein kinase in membranes with ANF-RGC (56). These studies were, and remain, the foundation of the role of ATP in ANF-RGC phosphorylation and consequently in ANF-RGC activation. The ordered sequence of these steps remained speculative, one group supporting the phosphorylation as the first and the critical step (44,56), the other, supporting the opposite: allosteric followed by phosphorylation (32,40). One study even proposed that ATP had no direct effect on ANF-RGC activation; it was an indirect effect going through the hypothetical protein kinase (59), and it was the sole ANF signaling mechanism of ANF-RGC (59).

With the introduction of the staurosporine probe, the riddle was partially solved (32). It was established that ATP is an allosteric modifier of ANF-RGC, that this step is independent of the phosphorylation step and that it causes the partial stimulation of ANF-RGC, about 50%. This study also demonstrated that it is the 50% component of the AMP-PNP-activated ANF-RGC that is mimicked by staurosporine in the stimulation of ANF-RGC.

In accordance with the last conclusion, AMP-PNP should duplicate the staurosporine-activation profile of ANF/ANF-RGC signaling, i.e., it should stimulate ANF-RGC-6A, the dephosphorylated form of ANF-RGC, to the same level as staurosporine does; and, also importantly, ATP and ATPγS should do the same, because the ANF-RGC-6A mutant can neither be phosphorylated nor thiophosphorylated. Thus, ANF-RGC-6A mutant should respond identically to AMP-PNP, ATP and ATPγS.

This reasoning was experimentally validated. The wt-ANF-RGC in the presence of 10^{-7} M ANF was stimulated 5-fold above basal level by AMP-PNP, 8-fold by ATP and 11-fold by ATPγS (Fig. 5A). The EC_{50} values were: 0.25, 0.20 and 0.15 mM for AMP-PNP, ATP and ATPγS, respectively (Fig. 5A). Similar EC_{50} values were obtained from Hill's plots calculated for each of the nucleotides: 0.22 mM for AMP-PNP, 0.2 mM for ATP and 0.16 mM for ATPγS (Hill's coefficient is 1 ±.0.2 for the wtANF-RGC dose-dependent

stimulation by AMP-PNP, ATP and ATPγS). These results demonstrated that the targeted site of ATP and its analogues action in the ARM domain of ANF-RGC is the same; the only difference resides in their effectiveness to saturate the ANF-RGC activity.

In contrast, the level and the profile of ATP and ATPγS stimulation of ANF-RGC-6A mutant became almost indistinguishable from that of AMP-PNP (Fig. 5B–D). Now, all three nucleotides—AMP-PNP, ATP, ATPγS—saturated ANF-RGC-6A to the comparable levels and their EC_{50} values were identical. The maximal stimulation of the ANF-RGC-6A mutant with AMP-PNP was 4.6 fold (Fig. 5B), with ATP 4.5 fold (Fig. 45), and with ATPγS, 4.6 fold (Fig. 5D); the EC_{50} values for all three nucleotides were 0.3 mM (0.27, 0.25 and 0.26 mM when calculated from Hill's plot for AMP-PNP, ATP and ATPγS dose-response curves, respectively).

To define the role of the individual six phosphorylated residues of the ARM, the ANF-RGC mutants--$S^{497}A$, $T^{500}A$, $S^{502}A$, $S^{506}A$, $S^{510}A$, $T^{513}A$--were exposed to 10^{-7} M ANF and increasing concentrations of ATP (Fig. 6). All of them were stimulated in an ATP-dose dependent fashion, however, the V_{max} reached by each mutant was different: The $S^{497}A$ mutant achieved only ~43% of the wt-ANF-RGC stimulated activity; $T^{500}A$, ~62%; $S^{502}A$, ~70%; $S^{506}A$ and $S^{510}A$, ~50%; and $T^{513}A$, ~75% (Fig. 6). Thus, the response varied from ~40% to ~75% of the wt-ANF-RGC response depending on the amino acid mutated. None of them, however, lost the ability to be stimulated by ANF/ATP. Even the most significantly lowered stimulated activity, observed for the $S^{497}A$ mutant, was within the range of activity reached by the wt-ANF-RGC in the presence of ANF and non-phosphorylating allosteric modulators, staurosporine and AMP-PNP. Together, these results validate the earlier conclusion that the allosterically modulated ANF stimulation does not require phosphorylation of the six residues.

These results dissect the two, allosteric and phosphorylation, modes of ATP effect, provide a compelling evidence that allosteric mode does not require phosphorylation. Alone, however, it is not sufficient to bring ANF-RGC to the fully activated state.

To further verify this conclusion ANF signaling of ANF-RGC was assessed in the simultaneous presence of both AMP-PNP and ATP in the reaction mixture. Two AMP-PNP and ATP concentrations were tested, 0.25 mM each (concentrations causing approx. half-maximal stimulation of ANF-RGC in the presence of 10^{-7} M ANF) and 1 mM each (the nucleotides concentrations at which the maximal stimulation of ANF-RGC occurs). The results are shown in figure 7. In the presence of 10^{-7} M ANF and 0.25 mM AMP-PNP or ATP the ANF-RGC activity was stimulated respectively 2.7- and 4.5-fold above the basal value; when AMP-PNP and ATP at the same concentrations were co-present in the reaction mixture, their stimulatory effect was almost additive, 6.3 ± 0.4 fold above the basal value. However, when the two nucleotides were co-present at concentrations causing maximal stimulation of ANF-RGC (1 mM of each), the stimulated activity was comparable to that caused by 1 mM ATP alone. These results confirm that the allosteric modification and phosphorylation are two independent signaling steps in ANF-RGC activation.

Together with the abundant prior evidences that G^{505} in the Grc motif of ARM (Fig. 1A) is a pivotal transduction component in the ATP signaling of ANF-RGC (51), the present study supports the observation that aided in construction of the ARM domain model (40). In this model, the ATP signaling, through allosteric modification pivots G^{505} and exposes S^{506} from its buried state (43). The present study suggests that ATP binding would also result in exposure of the other phosphorylated residues - S^{497}, T^{500}, S^{502}, S^{510}, T^{513}. Only then would it be possible for ANF-RGC to be phosphorylated and for ATP to exhibit its phosphorylation activity through a hypothetical protein kinase. In summary, the ATP

activation of the ARM is a dynamic and ordered event, allosteric step governing the phosphorylation step, and these two together, causing full saturation of the ANF-RGC activity.

Negative charges substituting phosphorylated residues mimic phosphorylation without fully restoring ANF-RGC activation

With the acquired information that ATP allosteric modification of the ARM domain is independent of the ATP phosphorylation step, the staurosporine probe was used to answer the next two critical questions: Does the phoshorylated state of ANF-RGC affect ATP-dependent (1) signaling of ANF-RGC activation; and (2) allosteric modification?

To answer these questions advantage was taken of a previous observation. Working on elucidation of the role of isocitrate dehydrogenase in the bacterial growth, the authors demonstrated that a negatively charged residue (aspartic acid) substituting serine of isocitrate dehydrogenase mimics its phosphorylated state (60). It inactivates the isocitrate dehydrogenase activity. This idea that the negative charge of the residue mimics the phophorylated state of the enzyme and its physiological activity has originally been instrumental to conclude that phoshorylation of ANF-RGC is the primary and the critical event in its ATP-dependent ANF signaling (44,45). These authors arrived at this conclusion through the studies where one residue, S^{497}, or all six--S^{497}, T^{500}, S^{502}, S^{506}, S^{510}, T^{513}-- were replaced with glutamic acid, resulting in the respective S^{497}E and ANF-RGC-6-E mutant (44,45). They concluded that negative charges were able to facilitate ANF signaling of ANF-RGC, thus, phosphorylation of ANF-RGC was the primary and critical signaling event of ANF-RGC activation (45).

With the availability of the staurosporine probe, the above concept was retested, using the ANF-RGC-6D mutant. In this mutant all six phoshorylated sites of ANF-RGC-- S^{497}, T^{500}, S^{502}, S^{506}, S^{510}, T^{513}--were replaced, according to (60) with aspartic acid (Fig. 1C). This mutant was then analyzed for its ATP-dependent ANF signaling activities: phosphorylation and allosteric modification.

The mutant was first analyzed for its active expression in the heterologous system of COS cells. It exhibited the basal activity of 4.1 pmol cyclic GMP formed $minute^{-1}$ mg^{-1} protein with the K_M of 476 μM for GTP. Thus, the mutant's expression and its basal biochemical characteristics were very similar to those of the wt- ANF-RGC.

Aspartate residues only partially facilitate ANF/ATP signaling of ANF-RGC— The ANF-RGC-6D mutant expressed in COS cells was exposed to 10^{-7} M ANF and the increasing concentrations of ATP, ATPγS, AMP-PNP or staurosporine. All these nucleotides and staurosporine, stimulated the guanylate cyclase activity of the mutant-ANF-RGC in a dose-dependent fashion. There were, however, two significant kinetic differences between the ANF-RGC-6D mutant and the wtANF-RGC. First, and the most dramatic, was that all nucleotides--ATP, ATPγS, AMP-PNP--stimulated ANF-RGC-6D to the same extent, 3.6-fold over the basal level while each of them stimulated wtANF-RGC to different extent (compare figures 8A–8C with figure 5A). This meant that the 6D mutation caused the V_{max} drop in their respective values of 56% (8.1- to 3.6-fold for ATP), 64% (10.1- to 3.6-fold for ATPγS) and 28% (5.0 to 3.6-fold for AMP-PNP) in ANF-RGC signaling activity. The drop in staurosporine activation was 22% (4.5- to 3.5-fold), as expected, almost identical to that observed with AMP-PNP.

Because, the mutant was equivalent in its responses to ATP and, most significantly, to AMP-PNP and staurosporine, it meant that the negative charges of the aspartic acid residues do, indeed, mimic the functional characteristics of their corresponding phosphorylated

residues-- S^{497}, T^{500}, S^{502}, S^{506}, S^{510}, T^{513}. Three important conclusions are drawn from these results: (1) ATP-dependent phosphorylation step contributes in ANF-RGC signaling yet, (2) this signaling is only partial; (3) since modulators without phosphorylation activity, staurosporine and AMP-PNP, can activate ANF-RGC, allosteric modification and not phosphorylation is the primary event in ANF-RGC signaling.

Second, phosphorylation of the ARM domain affects allosteric modification of ANF-RGC as evident from the observed sigmoidal profiles of the dose-response curves. Curve fitting using the Hill's equation yielded Hill's coefficient of 1.5 for AMP-PNP, 1.8 for ATP, 1.7 for ATPγS, and 1.3 for staurosporine. Thus, interaction of adenine nucleotides and staurosporine with ANF-RGC-6D mutant is cooperative, while it is non-cooperative with wt-ANF-RGC and its alanine mutants. Due to the cooperativity, the EC_{50} values were determined not directly from the dose-response curves but from the respective Hill's plots. They were 0.4 ± 0.05 mM for the adenine nucleotides and 0.15 μM for staurosporine. It is, thus, concluded that compared to the dephosphorylated, the phosphorylated form of ANF-RGC is less amenable to the ATP allosteric modification and activation, meaning phosphorylation converts ANF-RGC from high to low ATP-affinity form.

Direct analysis of the ARM domain for ATP binding validates this conclusion —Having ascertained that phosphorylation of ANF-RGC lowers its susceptibility to the ATP allosteric modification, this conclusion was tested by the direct ATP binding studies with its target ARM domain.

Three ARM constructs (aa 486–692), wt-ARM, ARM-6A, and ARM-6D were individually expressed and purified. In solution they existed as monomers as determined by FPLC (Experimental Procedures). It is in agreement with the existing biochemical, crystalographical and molecular modeling data showing that dimeric contact points between two ANF-RGC monomers are within the extracellular domain (34,35,61,62) and the catalytic domain (25).

The purified ARM domain proteins were cross-linked with [α^{32}P]-8-azido-ATP in the absence or presence of increasing concentrations of cold ATP. Reaction mixtures were resolved on SDS-PAGE, an X-ray film was exposed to the gel and the radioactive bands corresponding to the cross-linked ARM domains were identified. After the exposure, the gel was aligned with the autoradiogram, the radioactive bands were cut out from the gel and counted for radioactivity. The results are shown in figure 9.

In the absence of cold ATP the wt-ARM and the ARM-6A mutant bound approximately the same amount of [α^{32}P]-8-azido-ATP (~800 cpm) whereas the ARM-6D mutant bound only about half of that amount (~400 cpm). Increasing concentrations of cold ATP dose-dependently lowered the amount of [α^{32}P]-8-azido-ATP cross-linked with each of the ARM protein but with different efficiency. 0.5 mM cold ATP lowered by 50% the [α^{32}P]-8-azido-ATP cross-linked with the wt-ARM and the ARM-6A mutant but 1 mM ATP was necessary to obtain the same lowering with the ARM-6D mutant. These results demonstrate that compared to its non-phosphorylated form, the phosphorylated form of ARM domain has two-times lower affinity for ATP binding. They, thus, support the results obtained with full-length guanylate cyclases and explain the difference in the potency of ATP and its other analogues--ATPγS, AMP-PNP--and staurosporine in stimulation of ANF-RGC-6A and -6D mutants (*vide supra*).

Molecular modeling

To explain the biochemical results in 3-D terms the ARM domain model [PDB file 1T53 and (40)] was analyzed in its apo- and ATP bound states. The model represents one ATP

binding site within the ARM domain monomer what is consistent with the existing biochemical data (39,49). The analysis of the ARM domain model was focused on the six serine and threonine residues, the Grc motif, and their surroundings. These residues are located in the smaller, N-terminal lobe of the ARM domain and are a part of the S^{497}-T^{513} amino acid stretch forming the β1 and β2 strands and the connecting loop (40,42,43). G^{505} of the Grc motif is pivotally positioned at a junction of these two β strands (40,42,43). Except for L^{511} and T^{513}, which belong to the ATP binding pocket and are within the interacting distance with the adenine moiety of ATP, other residues of the S^{497}-T^{513} stretch do not interact directly with ATP (40,42,43), but they form the floor of the pocket that helps to stabilize the ATP binding. The model of the ARM domain is shown in figure 10 (the N-terminal lobe is in magenta, the β1 and β2 strands in blue, the positions of the serine and threonine residues are indicated and their side chains are shown, G^{505} is labeled in grey, the C-terminal lobe is in cyan, and the solvent accessible surface of ATP, in green).

ATP binding to the ARM domain enables the phosphorylation step to occur— The 3-dimensional structure of the ARM domain was analyzed to determine the effect of ATP binding on the steric arrangement of the six phosphorylation sites. The results are presented in figure 11 (for clarity only the analyzed residues are shown). In the basal state (before ATP binding) the OH group of side chains of T^{500}, S^{502}, S^{506} and T^{513} are stabilized in a position away from the protein surface (Fig. 11: conformation of the residues before ATP binding is shown in cyan). Although the OH groups of S^{497} and S^{510} in the basal state are directed toward the surface, they too are not accessible. A detailed analysis of the model indicates that they are shielded by the side chains of surrounding amino acids: the OH group of S^{497} is shielded by the side chains of L^{499} and Q^{517}, while that of S^{510}, by the side chain of R^{536}.

After ATP binds to the ARM domain, the β1, β2 strands, and the loop between them shifts by ~3–4 Å and rotates by ~15° (40,42,43). G^{505} is a critical pivot for both the shift and the rotation (40,42,43). This movement causes reorientation of the serines and threonines residues (Fig. 11: red colored residues). As a consequence, the side chains and the OH groups of T^{500}, S^{502}, S^{506} and T^{513} are now directed toward the protein surface (Fig. 11: compare the positions of the cyan- and red-colored OH groups). The change in the positions of the side chains is most drastic for the S^{502} and S^{506} residues. Although upon ATP binding there is no toward the surface reorientation of the S^{497} and S^{510} OH groups, the entire residues are shifted toward the surface (Fig. 11). These results show that it is only after ATP binds to the ARM domain that the hypothetical protein kinase can access the side chains of the six residues. Thus, the structural arrangement of the putative phosphorylable residues S^{497}, T^{500}, S^{502}, S^{506}, S^{510}, and T^{513} before and after ATP binding explains the biochemical results in 3-dimensional terms. This explanation is most vivid in the case of S^{506}. Analysis of the ARM domain model shows that ATP binding affects most drastically the position and conformation of S^{506} [Fig. 11: compare S^{506} in cyan (before ATP binding) and in red (after ATP binding)] and biochemical results show that its phosphorylation appears to be highly significant for the ANF/ATP-dependent activation of ANF-RGC. Therefore, the conclusion, that phosphorylation follows the ATP-dependent step of allosteric modification is sterically validated.

Surface characteristics of the dephosphorylated form of the ARM domain favor ATP binding—To explain the observation that the wt ARM domain and ARM-6A mutant bind ATP with similar affinity whereas the ARM-6D mutant's affinity for ATP is lower, the S^{497}, T^{500}, S^{502}, S^{506}, S^{510}, and T^{513} residues were substituted with A or D residues in both apo and ATP bound structures of the ARM domain and the ARM-6A and ARM-6D models were constructed. In each case the side chains were scanned to minimize bad contacts and optimize favorable interactions with the surrounding residues.

Because surface characteristics of a protein are the deciding factor in its interaction with other molecules, it was reasoned, that the same would apply for the ARM domain interaction with ATP molecule. Therefore, solvent accessible surface (Connoly surface) was generated for the wt ARM and its -6A and -6D mutants and the electrostatic potential for each protein surface was mapped. The results are presented in figure 12. For the wt ARM and ARM-6A the surface potentials are virtually indistinguishable. The electrostatic potential pattern is, however, strikingly different for the ARM-6D mutant. Here, a large patch of negative surface potential is observed within a region close to the ATP binding pocket (Fig. 12: ARM-6D region within the dashed ellipse; the cleft between two ARM domain lobes where the ATP binding site is located is indicated by an arrow). This negative surface potential impedes ATP access to the protein surface and, consequently, its interaction with the binding pocket. These results provide explanation for the lowered affinity of ATP to the ARM-6D mutant in comparison with the wt ARM and its 6A mutant and they support the conclusion that phosphorylation changes the state of the ARM domain from high to low affinity for ATP.

DISCUSSION

The existing dogma is “that phosphorylation of the KHD is absolutely required for hormone-dependent activation of NPR-A” (44,45). Because at that time no probe to dissect out the two ATP effects, phosphorylation and allosteric modification, in ANF-RGC activation was available, it was not possible to scrutinize the biochemical principles on which the dogma was based.

In view of the recent findings that phosphorylation of the ARM domain (KHD) and its allosteric modification are two individual steps in the process of ANF-RGC (NPR-A) activation (32), the primary objective of the present study was to analyze the relationship between these two steps. This objective was achieved through the judicial use of the available tools in analyzing the properties of the dephosphorylated and the phosphorylated forms of ANF-RGC and applying them to the 3D-simulated ARM domain models.

The phoshorylation sites reside on seven residues of ANF-RGC ARM domain (45,53,54) but only six of them are involved in the process of activation. They are: S^{497}, T^{500}, S^{502}, S^{506}, S^{510}, and T^{513} (Fig. 1A). Conversion of these residues to alanine results in the ANF-RGC-6A mutant, which can no longer be phosphorylated. Yet, this mutant undergoes ATP-dependent allosteric modification and gets activated (Figures 4A and 5B–5D). The activation is about 50% of the wt-ANF-RGC. Importantly, the extent of activation is equivalent for ATPγS and its non-phosphorylating structural anlogues, AMP-PNP and staurosporine. Also, EC_{50} values for all these effector agents are equal. Unequal effects observed between these agents for wt ANF-RGC activation are eliminated and are replaced by their equality.

These findings settle that (1) the ATP-dependent phosphorylation is not the primary event of ANF-RGC activation; (2) the primary event is ATP allosteric modification; (3) the contribution of the allosteric step to the enzyme activation is about 50% of the maximal activation; and (4) the allosteric step occurs independently of the phosphorylation step, which apparently contributes the remaining 50% of the enzyme activity.

The latter deduction was confirmed by transforming the wt-ANF-RGC to its phosphorylated-mimicking form. Six aspartic acid residues replaced the corresponding six phoshorylated sites of ANF-RGC, resulting in the ANF-RGC-6D mutant. The mutant’s basal activity and its substrate affinity for GTP remain unchanged. The modified enzyme responds almost identically to its effectors. The differential activation by ATP or ATPγS

from AMP-PNP or staurosporine observed for the wt ANF-RGC vanishes. The mutant, however, does not achieve fully saturated activity comparable to that of wt ANF-RGC. Thus, contrary to what happens to the isocitrate dehydrogenase enzyme (60), prior phosphorylation does not impart the full functional phenotype in ANF-RGC.

Identical conclusions were arrived at, independently, through modeling studies involving wt ARM domain and its -6A and -6D mutants.

Analysis of the wt ARM domain model in its apo and ATP bound states shows that the residues constituting the phosphorylation sites of ANF-RGC are distal to the ATP and its binding pocket. Their conformations, however, are governed by ATP. In ATP-free (basal) state the conformation of these residues is such that their OH groups are not freely accessible from the surface. It is only after ATP binding that the hydroxy groups are accessible from the surface thus susceptible to phosphorylation.

Until now, the unanswered question of the ATP-dependent allosteric modification of the ARM domain was: what causes ATP dissociation from that domain after its function as an allosteric modifier is done? The presented study provides answer to this question at both the functional and molecular levels. It is that ATP allosteric modification leads to phosphorylation of serine and threonine residues and upon their phoshorylations the affinity of ARM domain for ATP diminishes. This indicates that the phoshorylation step turns “OFF” the ATP signal by changing the ARM domain ATP binding affinity from high to low.

With the incorporation of the above information the recently proposed “Two Step activation of ANF-RGC” model (32) is now refined.

ATP-dependent 2-step activation model [figure 7 in (32)]

The ANF signal originates by the binding of one molecule of ANF to the extracellular dimer domain of ANF-RGC (34,35). The binding modifies the juxtamembrane region where the disulfide ^{423}Cys-Cys^{432} structural motif is a key element in this modification (34–36). The signal twists the transmembrane domain (38), induces a structural change in the ARM domain, and prepares it for the ATP activation (42). Step 1, ARM domain binds ATP to its pocket what leads to a cascade of temporal and spatial changes (32,39,41–43). They involve (1) shift in ATP binding pocket position by 3 to 4Å; and rotation of its floor by 15^{o}. G^{505} acts as a critical PIVOT for both the shift and the rotation; (2) movement by 2 to 7Å, but not the rotation of its β4 and β5 strands and its loop; and (3) movement of its αEF helix by 2 to 5Å. This movement exposes its hydrophobic motif, ^{669}WTAPELL^{675} motif, which facilitates its direct (or indirect) interaction with the catalytic module resulting in its partial, about 50%, activation (39). Step 2, the six phosphorylation sites are brought from their buried to the exposed state. Through ATP and a hypothetical protein kinase they get phosphorylated and the full activation (additional 50%) of ANF-RGC is achieved. Concomitantly, phosphorylation converts ATP binding site from the high to low affinity, ATP dissociates and ANF-RGC returns to its ground state.

Acknowledgments

The authors thank Mr. Dawid Wojtas for technical assistance in the purification of the ARM domain proteins and the cross-linking experiments and the reviewers for their constructive comments on the manuscript.

This study was supported by the National Institutes of Health, National Heart Lung and Blood Institute [grants HL084584 and HL084584S].

ABBREVIATIONS

AMP-PNP	adenylyl-imidodiphosphate
ANF-RGC	atrial natriuretic factor receptor guanylate cyclase
ATPγS	Adenosine-5'-O-(3-thio)- triphosphate

References

1. Paul, AK. Doctoral thesis. University of Tennessee; 1986. Particulate guanylate cyclase from adrenocortical carcinoma 494. Purification, biochemical and immunological characterization.
2. Paul AK, Marala RB, Jaiswal RK, Sharma RK. Coexistenc of guanylate cyclase and atrial natriuretic factor receptor in a 180-kD protein. Science 1987;235:1224–1226. [PubMed: 2881352]
3. Kuno T, Andersen JW, Kamisaki Y, Waldman SA, Chang LY, Saheki S, Leitman DC, Nakane M, Murad F. Co-purification of an atrial natriuretic factor receptor and particulate guanylate cyclase from rat lung. J Biol Chem 1986;261:5817–5823. [PubMed: 2871018]
4. Meloche S, McNicoll N, Liu B, Ong H, De Léan A. Atrial natriuretic factor R1 receptor from bovine adrenal zona glomerulosa: purification, characterization, and modulation by amiloride. Biochemistry 1988;27:8151–8158. [PubMed: 2852953]
5. Takayanagi R, Inagami T, Snajdar RM, Imada T, Tamura M, Misono KS. Two distinct forms of receptors for atrial natriuretic factor in bovine adrenocortical cells. Purification, ligand binding, and peptide mapping. J Biol Chem 1987;262:12104–12113. [PubMed: 2887565]
6. Chang MS, Lowe DG, Lewis M, Hellmiss R, Chen E, Goeddel DV. Differential activation by atrial and brain natriuretic peptides of two different receptor guanylate cyclases. Nature 1989;341:68–72. [PubMed: 2570358]
7. Duda T, Goraczniak RM, Sitaramayya A, Sharma RK. Cloning and expression of an ATP-regulated human retina C-type natriuretic factor receptor guanylate cyclase. Biochemistry 1993;32:1391–1395. [PubMed: 7679284]
8. Schulz S, Singh S, Bellet RA, Singh G, Tubb DJ, Chin H, Garbers DL. The primary structure of a plasma membrane guanylate cyclase demonstrates diversity within this new receptor family. Cell 1989;58:1155–1162. [PubMed: 2570641]
9. Schulz S, Green CK, Yuen PS, Garbers DL. Guanylyl cyclase is a heat-stable enterotoxin receptor. Cell 1990;63:941–948. [PubMed: 1701694]
10. Currie MG, Fok KF, Kato J, Moore RJ, Hamra FK, Duffin KL, Smith CE. Guanylin: an endogenous activator of intestinal guanylate cyclase. Proc Natl Acad Sci USA 1992;89:947–951. [PubMed: 1346555]
11. Hamra FK, Forte LR, Eber SL, Pidhorodeckyj NV, Krause WJ, Freeman RH, Chin DT, Tompkins JA, Fok KF, Smith CE, Duffin KL, Siegel NR, Currie MG. Uroguanylin: structure and activity of a second endogenous peptide that stimulates intestinal guanylate cyclase. Proc Natl Acad Sci USA 1993;90:10464–10468. [PubMed: 7902563]
12. Sharma RK. Membrane guanylate cyclase is a beautiful signal transduction machine: overview. Mol Cell Biochem 2010;334:3–36. [PubMed: 19957201]
13. Goraczniak RM, Duda T, Sitaramayya A, Sharma RK. Structural and functional characterization of the rod outer segment membrane guanylate cyclase. Biochem J 1994;302:455–461. [PubMed: 7916565]
14. Koch KW. Purification and identification of photoreceptor guanylate cyclase. J Biol Chem 1991;266:8634–8637. [PubMed: 1673683]
15. Koch KW, Duda T, Sharma RK. Ca(2+)-modulated vision-linked ROS-GC guanylate cyclase transduction machinery. Mol Cell Biochem 2010;334:105–115. [PubMed: 19943184]
16. Sharma RK, Duda T, Venkataraman V, Koch KW. Calcium-modulated mammalian membrane guanylate cyclase ROS-GC transduction machinery in sensory neurons: A universal concept. Res Trends Curr Top Biochem Res 2004;6:111–144.
17. Gibson AD, Garbers DL. Guanylyl cyclases as a family of putative odorant receptors. Annu Rev Neurosci 2000;23:417–439. [PubMed: 10845070]

18. Foster DC, Wedel BJ, Robinson SW, Garbers DL. Mechanisms of regulation and functions of guanylyl cyclases. Rev Physiol Biochem Pharmacol 1999;135:1–39. [PubMed: 9932479]
19. Dizhoor AM, Hurley JB. Regulation of photoreceptor membrane guanylyl cyclases by guanylyl cyclase activator proteins. Methods 1999;19:521–531. [PubMed: 10581151]
20. Duda T, Sharma RK. ONE-GC membrane guanylate cyclase, a trimodal odorant signal transducer. Biochem Biophys Res Commun 2008;367:440–445. [PubMed: 18178149]
21. Leinders-Zufall T, Cockerham RE, Michalakis S, Biel M, Garbers DL, Reed RR, Zufall F, Munger SD. Contribution of the receptor guanylyl cyclase GC-D to chemosensory function in the olfactory epithelium. Proc Natl Acad Sci USA 2007;104:14507–14512. [PubMed: 17724338]
22. Pertzev A, Duda T, Sharma RK. Ca(2+) Sensor GCAP1: A Constitutive Element of the ONE-GC-Modulated Odorant Signal Transduction Pathway. Biochemistry 2010;49:7303–7313. [PubMed: 20684533]
23. Duda T, Sharma RK. Distinct ONE-GC transduction modes and motifs of the odorants: Uroguanylin and CO(2). Biochem Biophys Res Commun 2010;391:1379–1384. [PubMed: 20026308]
24. Sun L, Wang H, Hu J, Han J, Matsunami H, Luo M. Guanylyl cyclase-D in the olfactory CO2 neurons is activated by bicarbonate. Proc Natl Acad Sci USA 2009;106:2041–2046. [PubMed: 19181845]
25. Venkataraman V, Duda T, Ravichandran S, Sharma RK. Neurocalcin delta modulation of ROS-GC1, a new model of Ca(2+) signaling. Biochemistry 2008;47:6590–6601. [PubMed: 18500817]
26. de Bold AJ. Atrial natriuretic factor: a hormone produced by the heart. Science 1985;230:767–770. [PubMed: 2932797]
27. de Bold AJ, de Bold ML. Determinants of natriuretic peptide production by the heart: basic and clinical implications. J Investig Med 2005;53:371–377.
28. Pandey KN. Biology of natriuretic peptides and their receptors. Peptides 2005;26:901–932. [PubMed: 15911062]
29. John SW, Krege JH, Oliver PM, Hagaman JR, Hodgin JB, Pang SC, Flynn TG, Smithies O. Genetic decreases in atrial natriuretic peptide and salt-sensitive hypertension. Science 1995;267:679–681. Erratum in: *Science* 267:1753. [PubMed: 7839143]
30. Lopez MJ, Wong SK, Kishimoto I, Dubois S, Mach V, Friesen J, Garbers DL, Beuve A. Salt-resistant hypertension in mice lacking the guanylyl cyclase-A receptor for atrial natriuretic peptide. Nature 1995;378:65–68. [PubMed: 7477288]
31. Kuhn M, Voss M, Mitko D, Stypmann J, Schmid C, Kawaguchi N, Grabellus F, Baba HA. Left ventricular assist device support reverses altered cardiac expression and function of natriuretic peptides and receptors in end-stage heart failure. Cardiovasc Res 2004;64:308–314. [PubMed: 15485690]
32. Duda T, Yadav P, Sharma RK. ATP allosteric activation of atrial natriuretic factor receptor guanylate cyclase. FEBS J 2010;277:2550–2563. [PubMed: 20553491]
33. Duda T, Goraczniak RM, Sharma RK. Site-directed mutational analysis of a membrane guanylate cyclase cDNA reveals the atrial natriuretic factor signaling site. Proc Natl Acad Sci USA 1991;88:7882–7886. [PubMed: 1679239]
34. Ogawa H, Qiu Y, Ogata CM, Misono KS. Crystal structure of hormone-bound atrial natriuretic peptide receptor extracellular domain: rotation mechanism for transmembrane signal transduction. J Biol Chem 2004;279:28625–28631. [PubMed: 15117952]
35. Ogawa H, Qiu Y, Huang L, Tam-Chang SW, Young HS, Misono KS. Structure of the atrial natriuretic peptide receptor extracellular domain in the unbound and hormone-bound states by single-particle electron microscopy. FEBS J 2009;276:1347–1355. [PubMed: 19187227]
36. Duda T, Sharma RK. Two membrane juxtaposed signaling modules in ANF-RGC are interlocked. Biochem Biophys Res Commun 2005;332:149–156. [PubMed: 15896311]
37. Huo X, Abe T, Misono KS. Ligand binding-dependent limited proteolysis of the atrial natriuretic peptide receptor: juxtamembrane hinge structure essential for transmembrane signal transduction. Biochemistry 1999;38:16941–16951. [PubMed: 10606529]

38. Parat M, Blanchet J, De Léan A. Role of juxtamembrane and transmembrane domains in the mechanism of natriuretic peptide receptor A activation. Biochemistry 2010;49:4601–4610. [PubMed: 20214400]
39. Duda T, Bharill S, Wojtas I, Yadav P, Gryczynski I, Gryczynski Z, Sharma RK. Atrial natriuretic factor receptor guanylate cyclase signaling: new ATP-regulated transduction motif. Mol Cell Biochem 2009;324:39–53. [PubMed: 19137266]
40. Duda T, Yadav P, Jankowska A, Venkataraman V, Sharma RK. Three dimensional atomic model and experimental validation for the ATP-Regulated Module (ARM) of the atrial natriuretic factor receptor guanylate cyclase. Mol Cell Biochem 2000;214:7–14. [PubMed: 11195792]
41. Duda T. Atrial natriuretic factor-receptor guanylate cyclase signal transduction mechanism. Mol Cell Biochem 2010;334:37–48. [PubMed: 19941036]
42. Duda T, Venkataraman V, Ravichandran S, Sharma RK. ATP-regulated module (ARM) of the atrial natriuretic factor receptor guanylate cyclase. Peptides 2005;26:969–984. [PubMed: 15911066]
43. Sharma RK, Yadav P, Duda T. Allosteric regulatory step and configuration of the ATP-binding pocket in atrial natriuretic factor receptor guanylate cyclase transduction mechanism. Can J Physiol Pharmacol 2001;79:682–691. [PubMed: 11558677]
44. Potter LR, Hunter T. Phosphorylation of the kinase homology domain is essential for activation of the A-type natriuretic peptide receptor. Mol Cell Biol 1998;18:2164–2172. [PubMed: 9528788]
45. Potter LR, Hunter T. A constitutively “phosphorylated” guanylyl cyclase-linked atrial natriuretic peptide receptor mutant is resistant to desensitization. Mol Biol Cell 1999;10:1811–1820. [PubMed: 10359598]
46. Potter LR, Abbey-Hosch S, Dickey DM. Natriuretic peptides, their receptors, and cyclic guanosine monophosphate-dependent signaling functions. Endocr Rev 2006;27:47–72. [PubMed: 16291870]
47. Sambrook, MJ.; Fritsch, EF.; Maniatis, T. Molecular Cloning: A Laboratory Manual. 2. Cold Spring Harbor Laboratory Press; Cold Spring Harbor, NY: 1989.
48. Nambi P, Aiyar NV, Sharma RK. Adrenocorticotropin-dependent particulate guanylate cyclase in rat adrenal and adrenocortical carcinoma: comparison of its properties with soluble guanylate cyclase and its relationship with ACTH-induced steroidogenesis. Arch Biochem Biophys 1982;217:638–646. [PubMed: 6127983]
49. Burczynska B, Duda T, Sharma RK. ATP signaling site in the ARM domain of atrial natriuretic factor receptor guanylate cyclase. Mol Cell Biochem 2007;301:193–207.
50. Chinkers M, Garbers DL, Chang MS, Lowe DG, Chin HM, Goeddel DV, Schulz S. A membrane form of guanylate cyclase is an atrial natriuretic peptide receptor. Nature 1989;338:78–83. [PubMed: 2563900]
51. Goraczniak RM, Duda T, Sharma RK. A structural motif that defines the ATP-regulatory module of guanylate cyclase in atrial natriuretic factor signalling. Biochem J 1992;282:533–537. [PubMed: 1347681]
52. Potter LR, Hunter T. Identification and characterization of the major phosphorylation sites of the B-type natriuretic peptide receptor. J Biol Chem 1998;273:15533–15539. [PubMed: 9624142]
53. Schröter J, Zahedi RP, Hartmann M, Gassner B, Gazinski A, Waschke J, Sickmann A, Kuhn M. Homologous desensitization of guanylyl cyclase A, the receptor for atrial natriuretic peptide, is associated with a complex phosphorylation pattern. FEBS J 2010;277:2440–2453. [PubMed: 20456499]
54. Yoder AR, Stone MD, Griffin TJ, Potter R. Mass Spectrometric Identification of Phosphorylation Sites in Guanylyl Cyclase A and B. Biochemistry. 2010 epub Nov 8.
55. Potter LR, Hunter T. Identification and characterization of the phosphorylation sites of the guanylyl cyclase-linked natriuretic peptide receptors A and B. Methods 1999;19:506–520. [PubMed: 10581150]
56. Foster DC, Garbers DL. Dual role for adenine nucleotides in the regulation of the atrial natriuretic peptide receptor, guanylyl cyclase-A. J Biol Chem 1998;273:16311–16318. [PubMed: 9632692]
57. Marala RB, Sitaramayya A, Sharma RK. Dual regulation of atrial natriuretic factor-dependent guanylate cyclase activity by ATP. FEBS Lett 1991;281:73–76. [PubMed: 1673103]

58. Chinkers M, Singh S, Garbers DL. Adenine nucleotides are required for activation of rat atrial natriuretic peptide receptor/guanylyl cyclase expressed in a baculovirus system. J Biol Chem 1991;266:4088–4093. [PubMed: 1671858]

59. Antos LK, Abbey-Hosch SE, Flora DR, Potter LR. ATP-independent activation of natriuretic peptide receptors. J Biol Chem 2005;280:26928–26932. [PubMed: 15911610]

60. Thorsness PE, Koshland DE Jr. Inactivation of isocitrate dehydrogenase by phosphorylation is mediated by the negative charge of the phosphate. J Biol Chem 1987;262:10422–10425. [PubMed: 3112144]

61. De Léan A, McNicoll N, Labrecque J. Natriuretic peptide receptor A activation stabilizes a membrane-distal dimer interface. J Biol Chem 2003;278:11159–11166. [PubMed: 12547834]

62. Parat M, McNicoll N, Wilkes B, Fournier A, De Léan A. Role of extracellular domain dimerization in agonist-induced activation of natriuretic peptide receptor A. Mol Pharmacol 2008;73:431–440. [PubMed: 17965196]

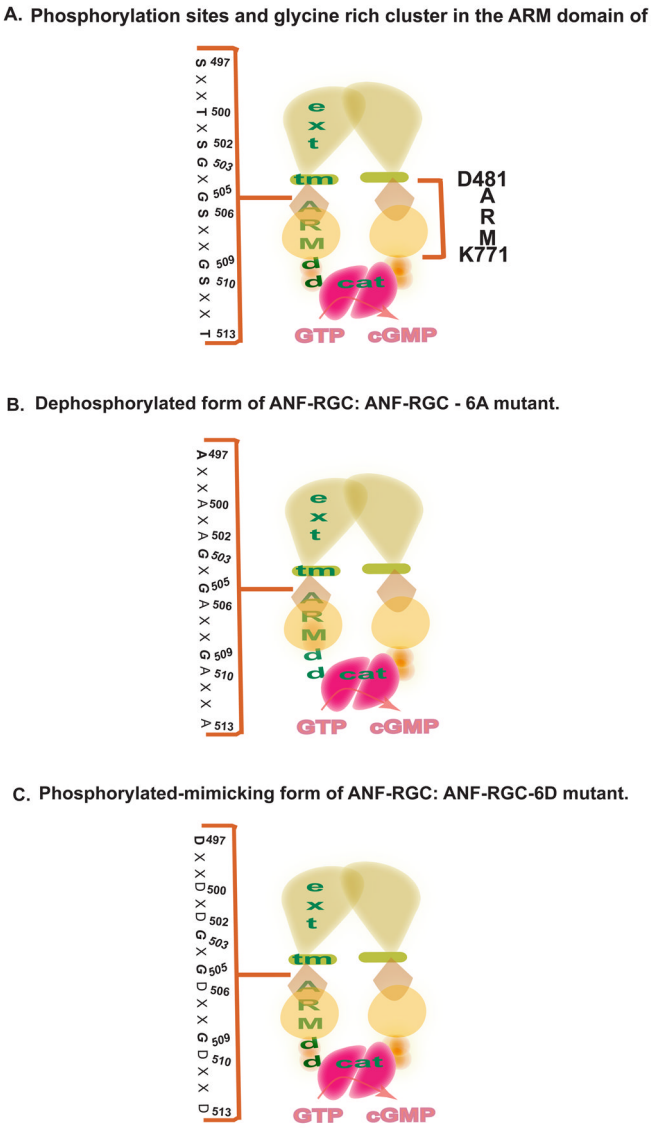

Figure 1. Modular structure of ANF-RGC

The functional domains of ANF-RGC are denoted as: ext, extracellular domain; tm, transmembrane domain; ARM, ATP regulatory domain; dd, dimerization domain; cat, catalytic domain. The boundaries of the ARM domain are indicated to the right. **A. Activation-related phosphorylation sites and the glycine rich cluster in the ARM domain.** The localization of the six phosphorylation sites in ANF-RGC involved in the process of its activation (four serine residues: S^{497}, S^{502}, S^{506}, S^{510} and two threonine residues: T^{500}, T^{513}) and of the glycine rich cluster (G^{503}, G^{505} G^{509}) is shown. **B. Representation of the ANF-RGC-6A mutant.** The six phosphorylated amino acid residues were mutated to alanine. The mutant constitutes the permanently dephosphorylated form of ANF-RGC. **C. Representation of the ANF-RGC-6D mutant.** The six phosphorylated amino acid residues were mutated to aspartic acid. The mutant mimicks the phosphorylated form of ANF-RGC.

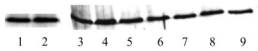

Figure 2. Expression of ANF-RGC and its alanine mutants in the membranes of COS cells

COS cells were transfected with wt ANF-RGC, its 6A mutant, or its single A mutants' cDNA. 72 hr after transfection the cells were harvested and their particulate fractions were prepared as described in "Materials and Methods". The membranes were analyzed by Western blotting using antibodies against ANF-RGC. Lane 1, wt ANF-RGC; Lane 2, ANF-RGC-6A mutant; Lane 3, wt ANF-RGC; Lane 4, ANF-RGC-S^{497}A; Lane 5, ANF-RGC-T^{500}A; Lane 6, ANF-RGC-S^{502}A; Lane 7, ANF-RGC-S^{506}A; Lane 8, ANF-RGC-S^{510}A; Lane 9, ANF-RGC-T^{513}A.

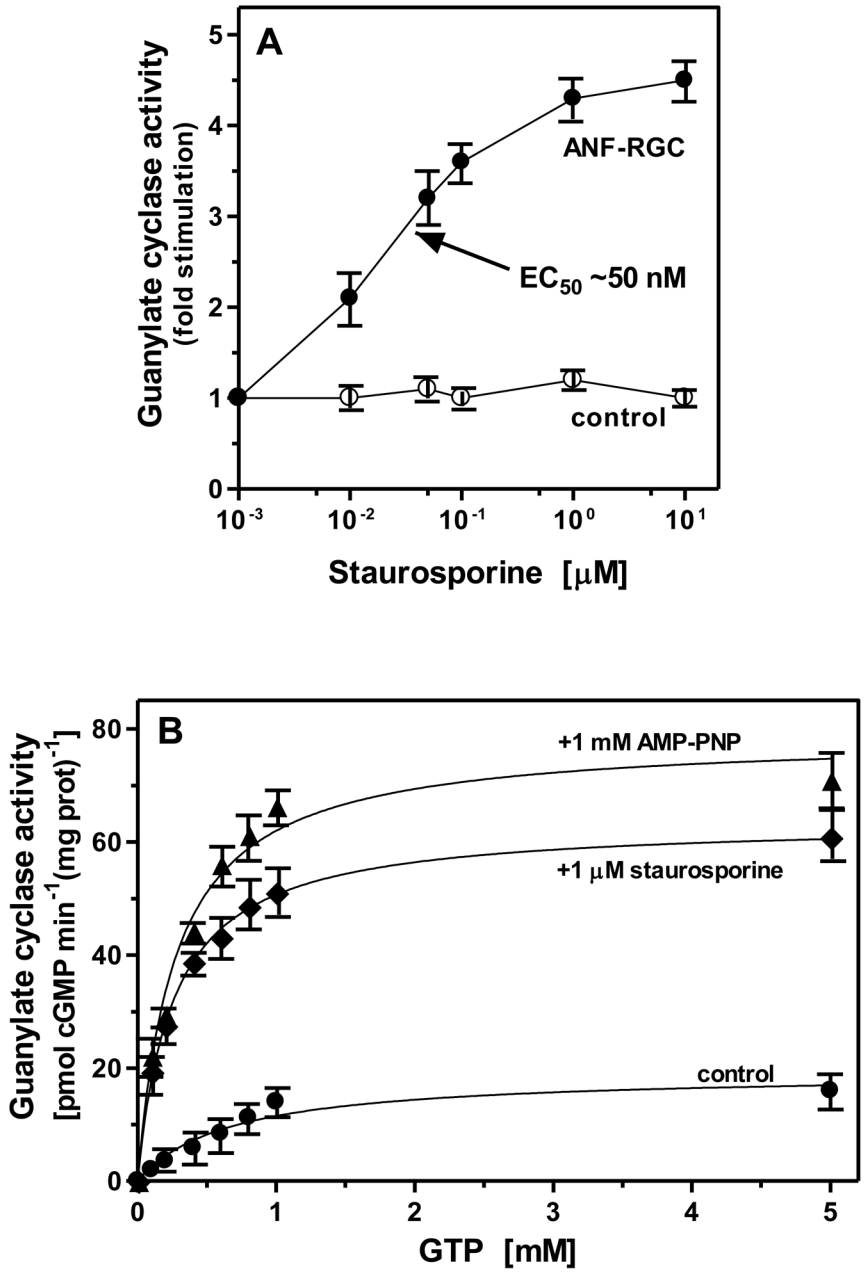

Figure 3.

(A) Effect of staurosporine on ANF-dependent activity of wt ANF-RGC. Membranes of COS cells transiently expressing ANF-RGC were analyzed for guanylate cyclase activity in the absence or presence of 10^{-7} M ANF and indicated concentrations of staurosporine. Membranes of "mock" transfected cells (control) were analyzed in parallel. The experiment was done in triplicate and repeated 6 times with separate preparations of transfected COS cells membranes. **(B) Effect of staurosporine and AMP-PNP on K_m of ANF-RGC.** Membranes of COS cells transiently expressing ANF-RGC were analyzed for guanylate cyclase activity with or without 1 mM staurosporine or 1 mM AMP-PNP in the presence of 10^{-7} M ANF and indicated concentrations GTP. The experiment was done in triplicate and repeated two times with separate COS membranes preparations. The results shown are mean ± SD from these experiments.

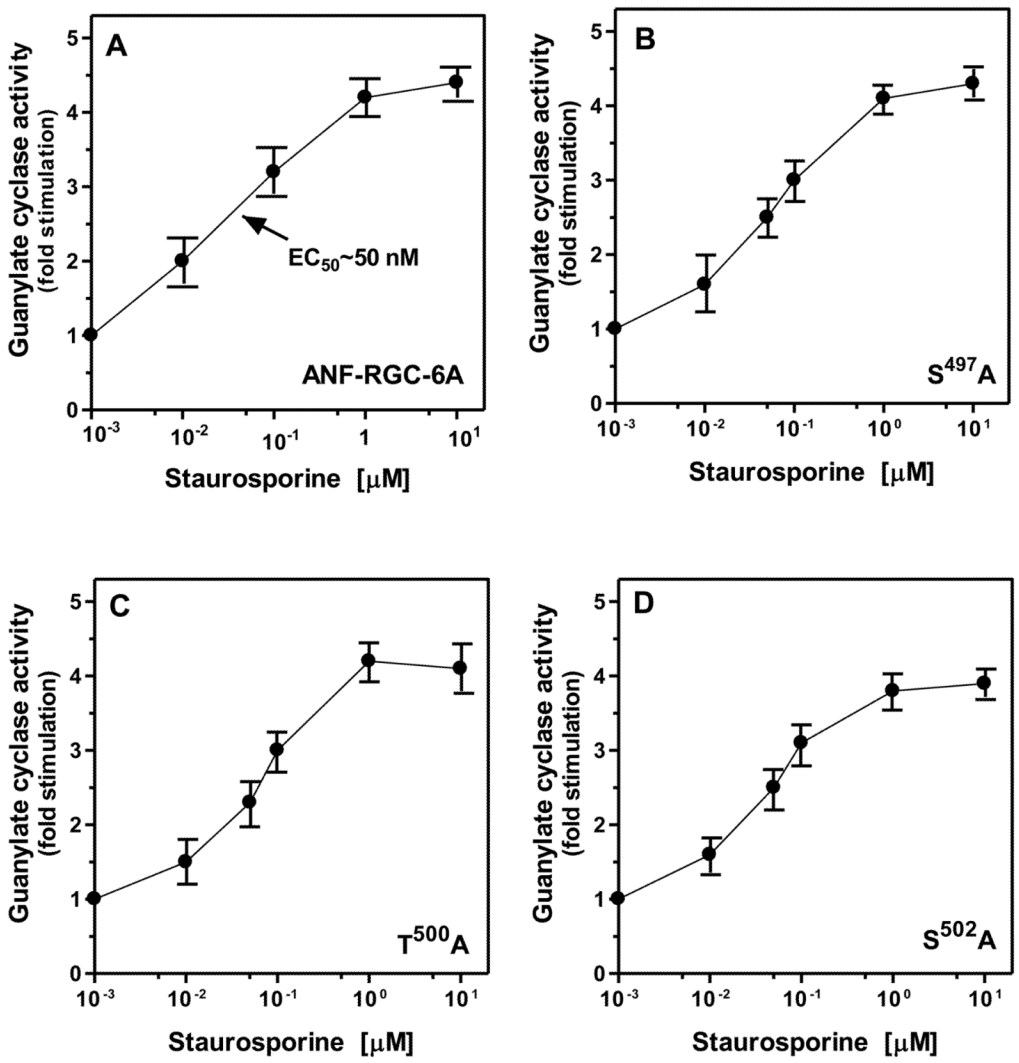

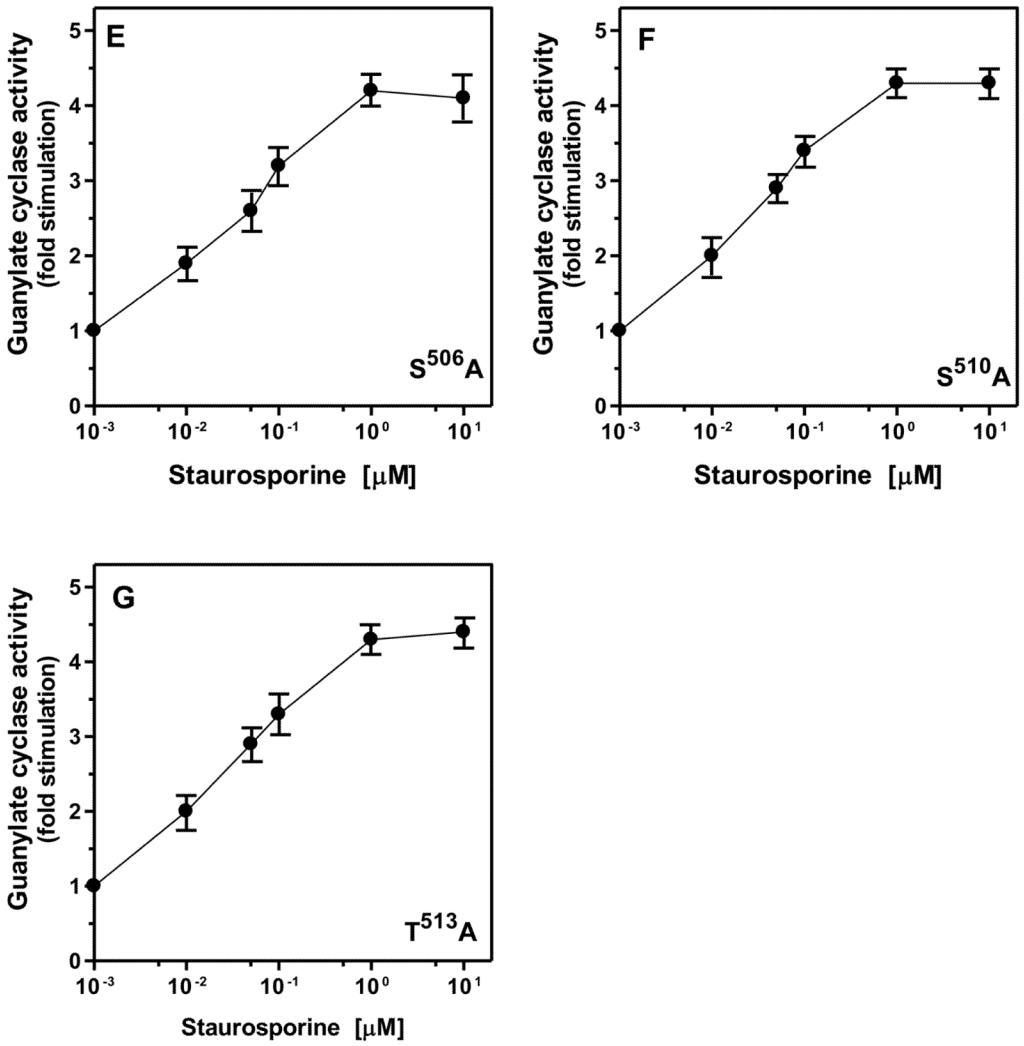

Figure 4. Effect of staurosporine on ANF-dependent activity of ANF-RGC-6A mutant (A) and six ANF-RGC mutants with single A mutations (B–G)

Membranes of COS cells transiently expressing the ANF-RGC-6A mutant or ANF-RGC single A mutants were analyzed for guanylate cyclase activity in the absence or presence of 10^{-7} M ANF and indicated concentrations of staurosporine. Membranes of "mock" transfected cells (control) were analyzed in parallel. Experiment was repeated 6 times with separate preparations of transfected COS cells membranes. The results presented are mean ± SD from these experiments.

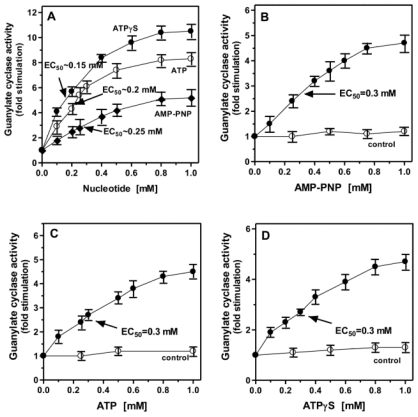

Figure 5. Effect of adenine nucleotides on ANF-dependent activation of ANF-RGC (A) and its 6A mutant (B–D)

Membranes of COS cells transiently expressing ANF-RGC or its 6A mutant were analyzed for guanylate cyclase activity in the absence or presence of 10^{-7} M ANF and indicated concentrations of adenine nucleotides, AMP-PNP, ATP or ATPγS. Membranes of "mock" transfected cells were analyzed in parallel (control). Experiment was repeated 6 times with separate preparations of transfected COS cells membranes. The results presented are mean ± SD from these experiments.

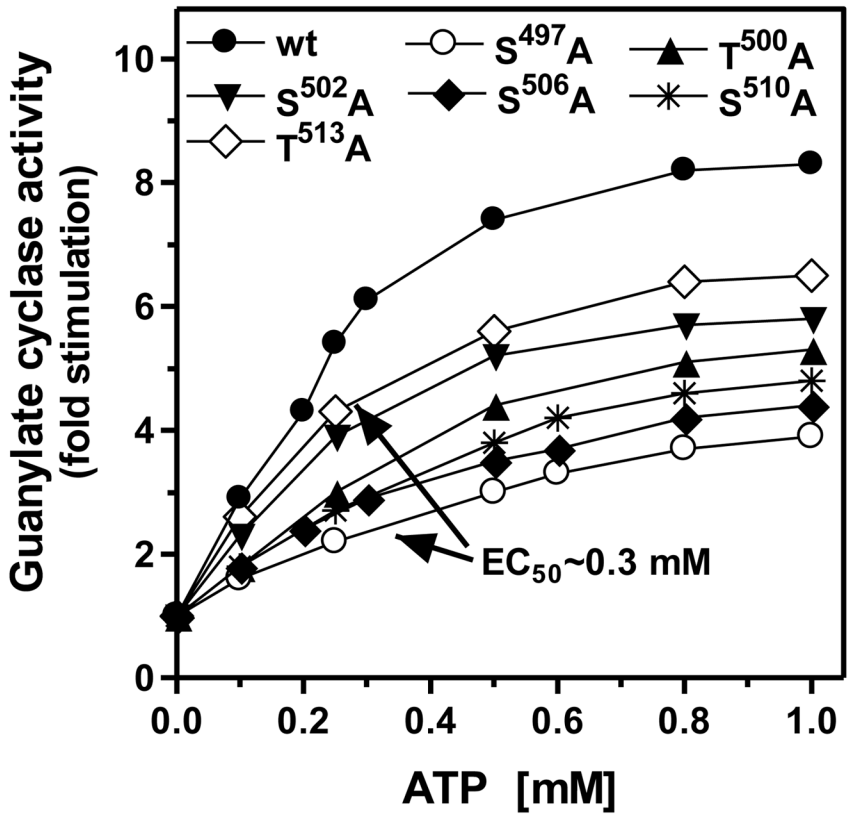

Figure 6. ATP effect on ANF-dependent activation of wt ANF-RGC and its six single A mutants

Membranes of COS cells transiently expressing ANF-RGC or its single A mutants: $S^{497}A$, $T^{500}A$, $S^{502}A$, $S^{506}A$, $S^{510}A$, $T^{513}A$ were analyzed for guanylate cyclase activity in the absence or presence of 10^{-7} M ANF and indicated concentrations of ATP. The results obtained with membranes of "mock" transfected cells were identical to those in figure 5C. Experiment was repeated 6 times with separate preparations of transfected COS cells membranes. The results presented are mean ± SD from these experiments.

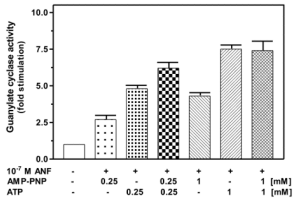

Figure 7. Combined effect of AMP-PNP and ATP on ANF-dependent activation of wt ANF-RGC

Membranes of COS cells transiently expressing ANF-RGC were analyzed for guanylate cyclase activity in the presence of 10^{-7} M ANF and indicated concentrations of AMP-PNP, ATP or AMP-PNP and ATP. Experiment was repeated 2 times with separate preparations of transfected COS cells membranes. The results presented are mean ± SD from these experiments.

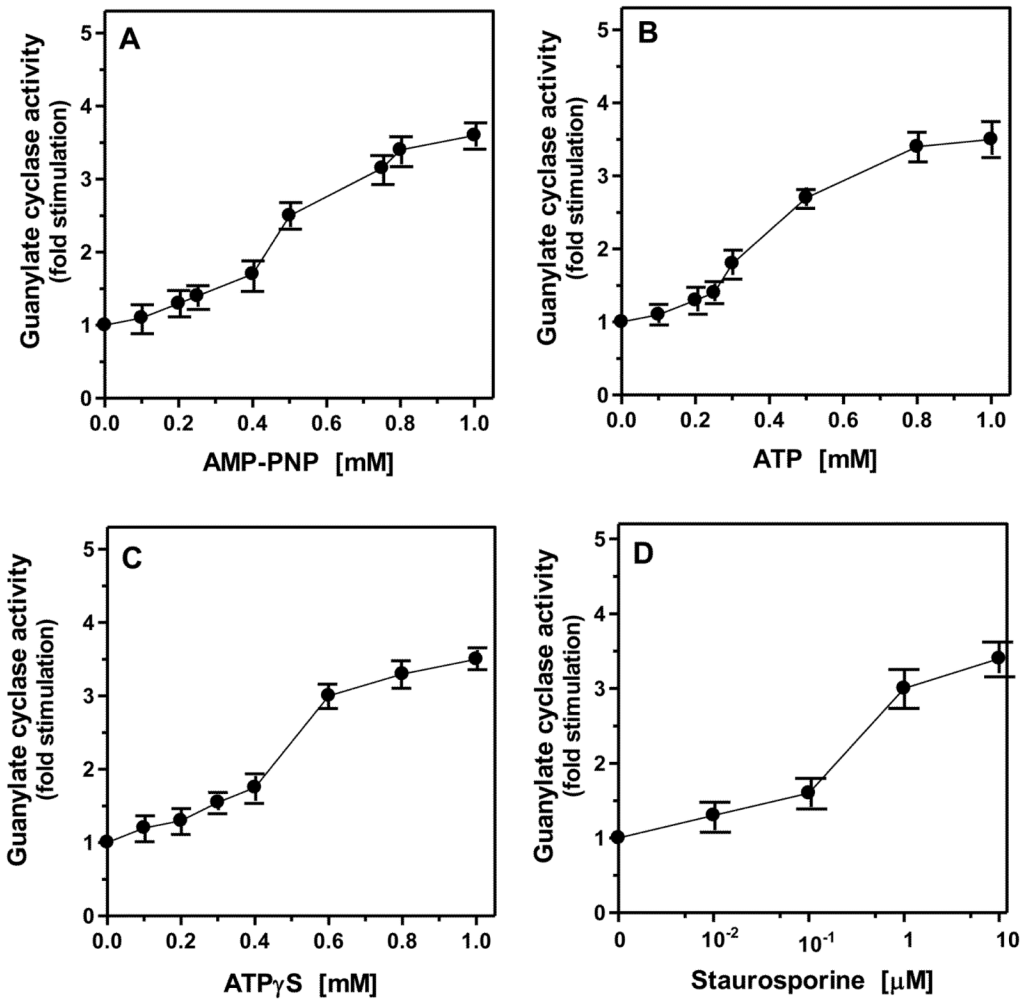

Figure 8. Effect of adenine nucleotides or staurosporine on ANF-dependent activation of ANF-RGC-6D mutant (A–D)

Membranes of COS cells transiently expressing the ANF-RGC-6D mutant were analyzed for guanylate cyclase activity in the absence or presence of 10^{-7} M ANF and indicated concentrations of adenine nucleotides, AMP-PNP, ATP, and ATPγS or staurosporine. The results obtained with membranes of "mock" transfected cells were identical to those shown in figures 4 and 5. Experiment was repeated 6 times with separate preparations of transfected COS cells membranes. The results presented are mean ± SD from these experiments normalized to ANF-RGC activity shown in figures 3A and 5A.

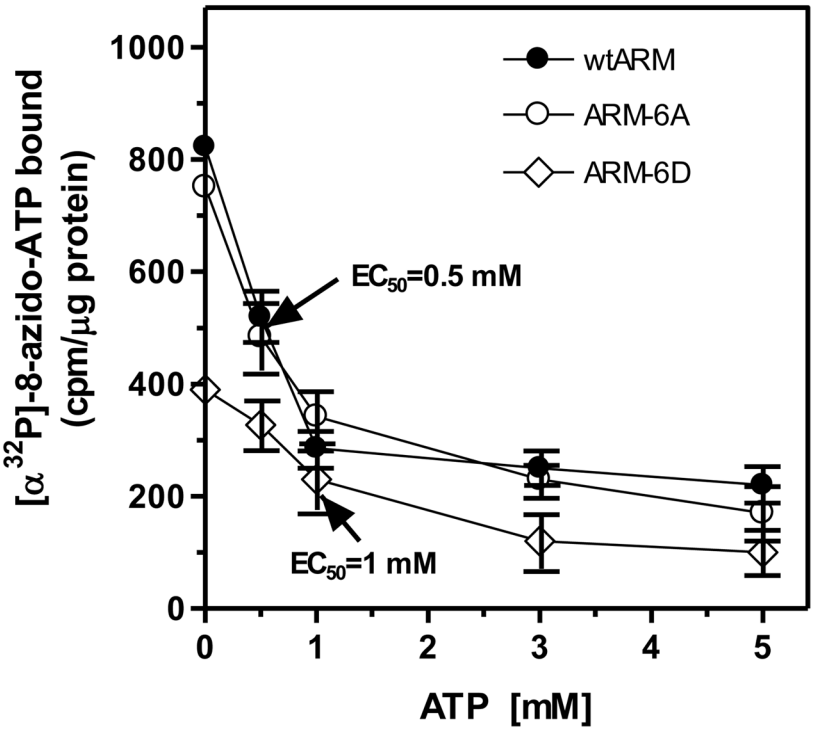

Figure 9. ATP binding to the ARM domain of ANF-RGC or its 6A or 6D mutants

The ARM domain fragment aa 486–692 of ANF-RGC or its 6A or 6D mutants was expressed and purified as described in "Experimental Procedures". The purified proteins were individually cross-linked with [α^{32}P]-8-azido-ATP in the absence or presence of indicated concentrations of ATP. The reactions mixtures were resolved on SDS-PAGE, the radioactive bands were excised from the gel and counted for radioactivity. The experiment was repeated 8 times with different preparations of ARM domain proteins. The results (mean ± SD) shown are from six of these experiments, the patterns from the remaining two were the same.

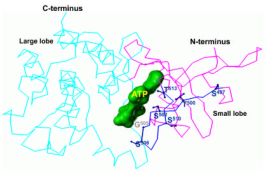

Figure 10. Model of the wt ANF-RGC ARM domain

The ANF-RGC ARM domain consists of two lobes. The smaller, N-terminal lobe is shown in magenta. The six putative activation-linked phosphorylation sites of ANF-RGC are located within the β1 and β2 strands of this lobe. The strands are shown in blue, the positions of six phosphorylation sites (S^{497}, T^{500}, S^{502}, S^{506}, S^{510} and T^{513}) are indicated and their side chains are shown. The position of G^{505} of Grc is also indicated. The larger, C-terminal lobe of the ARM domain is shown in cyan. ATP (green) binds to its pocket located in the cleft between the two lobes.

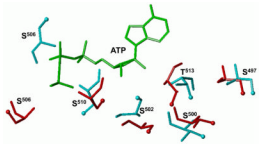

Figure 11. ATP binding to the ARM domain affects the conformation of the phosphorylable residues

The conformation of the six phosphorylated residues is shown before (cyan) and after (red) ATP binding. The ATP molecule is shown in green. The positions of the OH groups are indicated by cyan and red balls.

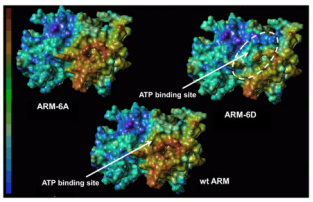

Figure 12. Electrostatic potentials at the surface of the wt-ARM domain and its 6A and 6D mutants

The phosphorylable residues (S^{497}, T^{500}, S^{502}, S^{506}, S^{510} and T^{513}) of the ARM domain were mutated to alanine or aspartate resulting in the construction of ARM-6A and ARM-6D models. The models were analyzed for the distribution of the electrostatic potentials at the surface of the ARM domain was analyzed using the SYBYL program as described in Experimental Procedures. The most significant changes of the potential were observed in the region of the cleft between the two lobes where ATP binds. This region is indicated by a dashed ellipse and the location of the ATP binding pocket is indicated by an arrow. The panel on the left provides a color ramp to indicate the range from the most negative (blue) to the most positive (brown) surface potential.

Table 1
Basic enzymatic characteristics of wt-ANF-RGC and its Alanine mutants

Wt-ANF-RGC and its alanine mutants were expressed in COS cells and their membranes were assayed for guanylate cyclase activity in the presence of varying concentrations (0- 1 mM) GTP and 5 mM $MgCl_2$. Experiment was done in triplicate and repeated two times. The results are mean ± SD from these experiments.

Cyclase	K_m [μM]	V_{max} [pmol cG/min/mg prot]
ANF-RGC	500 ± 28	6.2 ± 0.6
ANF-RGC-6A	485 ± 18	6.3 ± 0.4
ANF-RGC-S^{497}A	480 ± 25	5.6 ± 0.5
ANF-RGC-T^{500}A	490 ± 40	6.1 ± 0.5
ANF-RGC-S^{502}A	500 ± 38	5.8 ± 0.3
ANF-RGC-S^{506}A	490 ± 20	4.3 ± 0.4
ANF-RGC-S^{510}A	490 ± 35	5.1 ± 0.3
ANF-RGC-T^{513}A	510 ± 30	5.9 ± 0.4